Chaos Synchronization and Chaos Anticontrol of a Rotationally Supported Simple Pendulum*

Zheng-Ming GE**, Chia-Yang YU** and Yen-Sheng CHEN**

Chaos synchronization and anticontrol of a rotationally supported simple pendulum was studied in this paper. Different kinds of coupling terms are used to synchronize the two identical chaotic systems with different initial conditions. An observed-based scheme is also used to achieve synchronization. The results are demonstrated by phase portrait, Lyapunov exponent, Poincaré maps and synchronization time. Next, in order to analyze the transient behavior of the synchronized systems, Euclidean distance is used to plot a figure with coupling strength versus the distance. The chaotic signals are used to mask the message function in the secure communication system. Finally, anticontrol of chaos is achieved by adding constant term, periodic term, impulse term, time-delay term and adaptive control.

Key Words: Chaos, Synchronization, Anticontrol, Pendulum

1. Introduction

There has been growing interest in the investigation of chaos synchronization in the physical, mechanical, electrical, optical and biological field[1]-[3]. Chaos synchronization has been achieved by some approaches. The research has been motivated by this concept and has demonstrated some potential for using chaos in real-world applications such as secure communication and information processing[4].

In this paper, chaos synchronization and chaos anticontrol of a rotationally supported simple pendulum are researched. In Chapter 2, two identical chaotic systems are synchronized by adding different kinds of coupling terms. An observed-based scheme is also used to achieve synchronization[5]. Euclidean distance is used to analyze the influence to transient behavior of the synchronized systems[6]. In Chapter 3, we demonstrate the application of chaos synchronization by a new secure communication system[7]. In Chapter 4, anticontrol of chaos by adding different kinds of terms is used to enhance the chaotic range. Finally, adaptive control is also adopted for the same purpose to control systems from periodic motion to chaotic systems.

* Received 18th July, 2002 (No. 02-5102)

** Department of Mechanical Engineering, Nation Chiao Tung University, 1001 Ta Hsueh Road, Hsinchu 30050, Taiwan, Republic of China. E-mail: zmg@cc.nctu.edu.tw

2. Chaos Synchronization for the Coupled Systems

2.1 Description of the system model and differential equations of motion

The physical system considered here is depicted in Fig. 1. It is a pendulum suspended on a rotating

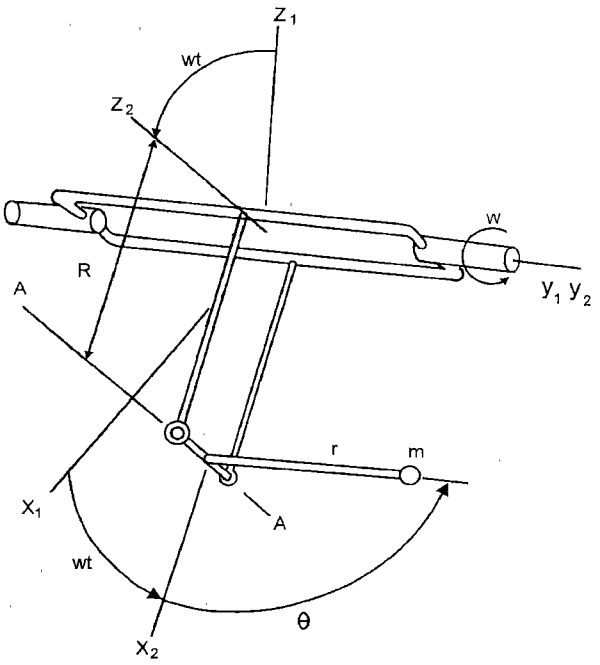

Fig. 1 The pendulum on rotating arm

arm system. The shaft rotates about the y_1-axis with the angular rate ω. The pendulum is pivoted (axis $A-A$) on an arm rigidly attached to the shaft. This rotation of the pendulum is described by the angle θ. The gravitational vector is in the negative z_1-direction. The length of the arm is R and the length of the pendulum is r. The motion is described by Lagrange's equation:

$$mr^2\frac{d^2\theta}{dt^2}+c_r\frac{d\theta}{dt}+\sin\theta(mRr\omega^2+mr^2\omega^2\cos\theta+mrg\sin\omega t)=0 \quad (1)$$

where ω is the angular rate of the shaft, c_r is the damping coefficient, g is the gravitational constant, m is the mass of the pendulum, r is the length of the pendulum, R is the length of the arm which is the distance from the pivot to the center of the shaft. The system Eq.(1) can be expressed in the form:

$$\frac{d^2\theta}{dt^2}+2\xi\frac{d\theta}{dt}+\sin\theta[\omega^2(\rho+\cos\theta)+\gamma\sin\omega t]=0 \quad (2)$$

where $2\xi=\frac{c_r}{mr^2}$, $\rho=\frac{R}{r}$, $\gamma=\frac{g}{r}$. Let $\theta=x_1$, $\dot{\theta}=x_2$, the state equations of the system can be written as:

$$\begin{cases}\dot{x}_1=x_2\\ \dot{x}_2=-2\xi x_2-\sin x_1[\omega^2(\rho+\cos x_1)+\gamma\sin\omega t]\end{cases} \quad (3)$$

The parameter values and initial conditions in Eq. (2) are $(\xi, \omega, \rho, \gamma)=(0.2, 2.0, 0.5, 14.3)$ and $(\theta(0), \dot{\theta}(0))=(\pi+0.02, 0.02)$.

2.2 Chaos synchronization of unidirectional coupled systems

2.2.1 Coupling by linear term In this subsection, we consider that two identical unidirectional-coupled systems are the drive (master) system $X=(x_1, x_2)$ and the response (slave) system $(Y(y_1, y_2)$. Two subsystems begin with two different initial conditions that will be synchronized by adding a linear coupling term. The systems can be expressed as

$$\begin{cases}\dot{x}_1=x_2\\ \dot{x}_2=-2\xi x_2-\sin x_1[\omega^2(\rho+\cos x_1)+\gamma\sin\omega t]\end{cases} \quad \text{(drive system)} \quad (4)$$

$$\begin{cases}\dot{y}_1=y_2\\ \dot{y}_2=-2\xi y_2-\sin y_1[\omega^2(\rho+\cos y_1)+\gamma\sin\omega t]\\ +k(x_1-y_1)\end{cases} \quad \text{(response system)} \quad (5)$$

where k is the coupling strength. The two identical systems have different initial conditions, which are $(x_1(0), x_2(0))=(\pi+0.02, 0.02)$, $(y_1(0), y_2(0))=(3, 0.05)$. The error dynamics is expressed by $e_i=x_i-y_i$, $(i=1, 2)$. When $k<8.35$, the two systems are not synchronized. When $k\geq 8.35$, the two systems begin to be synchronized, and the error dynamics approaches to zero finally.

Figure 2 shows the simulated results. When $k=8.35$, two systems are synchronized. The phase portraits of two subsystems are the same, and the error dynamics approaches to zero finally. The critical coupling strength k is 8.35.

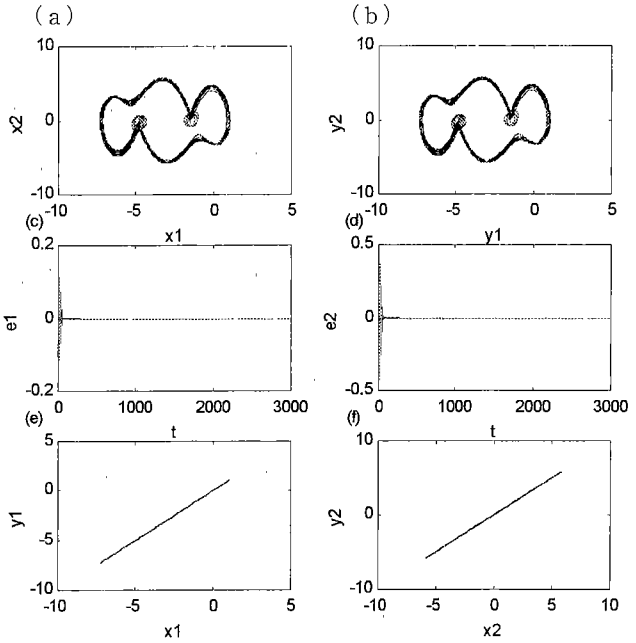

Fig. 2 (a), (b) Phase portrait, (c), (d) Time-response error and (e), (f) $x-y$ diagram of coupled systems with $k(x_1-y_1)$ for $k=8.35$

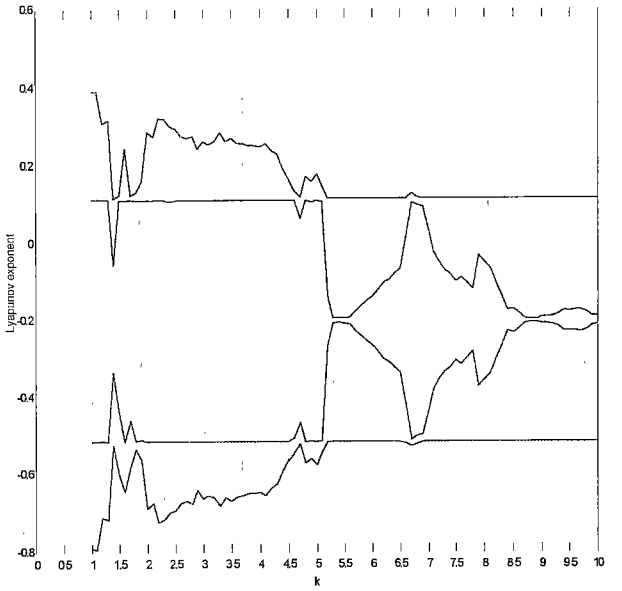

Fig. 3 The Lyapunov exponent of coupled systems with $k(x_1-y_1)$ for k between 0 and 10

We use the Lyapunov exponent method to detect the synchronization situation. In Fig. 3, the second Lyapunov exponent is negative in the synchronization region $k>8.35$. At the critical value about $k=8.35$, it approaches to zero and then becomes immediately negative again[8]. The results assist us in confirming

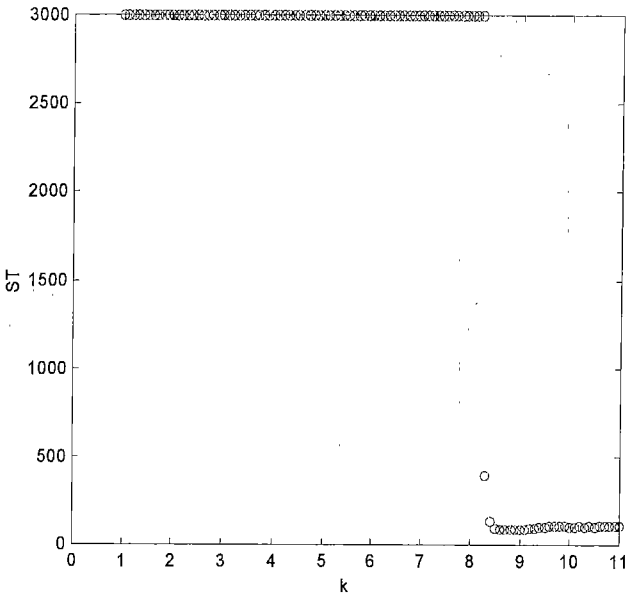

Fig. 4 Synchronization time for different k of the coupled systems with $k(x_1-y_1)$ coupling term

the accuracy of critical coupling strength. To study the efficacy of the synchronization strategy, we numerically computed the value of k for which stable synchronization is achieved, and its dependence on synchronization time ($ST=t_{syn}-t_0$)[9], where t_{syn} is the time at which the feedback terms are switched when the error signal $E(t)$ is less than 10^{-6}, and t_0 is the initial time. The error signal $E(t)$ is defined as:

$$E(t)=|x_1-y_1|+|x_2-y_2|+\frac{d}{dt}(|x_1-y_1|)+\frac{d}{dt}(|x_2-y_2|)$$

When coupling strength is larger, synchronization time is smaller. It can also assist us in confirming the accuracy of critical coupling strength. The result of the system is shown in Fig. 4

2.3 Observed-based synchronization scheme

Besides adding a coupling term, observed-based synchronization scheme can be used[5]. In the observed-based synchronization scheme, one (or more) signal of the drive system is used to substitute one (or more) variable in the response system. In this section, the drive system can be expressed as:

$$\begin{cases}\dot{x}_1=x_2\\ \dot{x}_2=-2\xi x_2-\sin x_1[\omega^2(\rho+\cos x_1)+\gamma\sin\omega t]\end{cases}$$

(drive system) (6)

A signal x_1 of the drive system is used to substitute the signal y_1 of the $\cos y_1$ term of the response system. Then the response system can be expressed as

$$\begin{cases}\dot{y}_1=y_2\\ \dot{y}_2=-2\xi y_2-\sin y_1[\omega^2(\rho+\cos x_1)+\gamma\sin\omega t]\end{cases}$$

(response system) (7)

Figure 5 shows the simulated result, two systems are

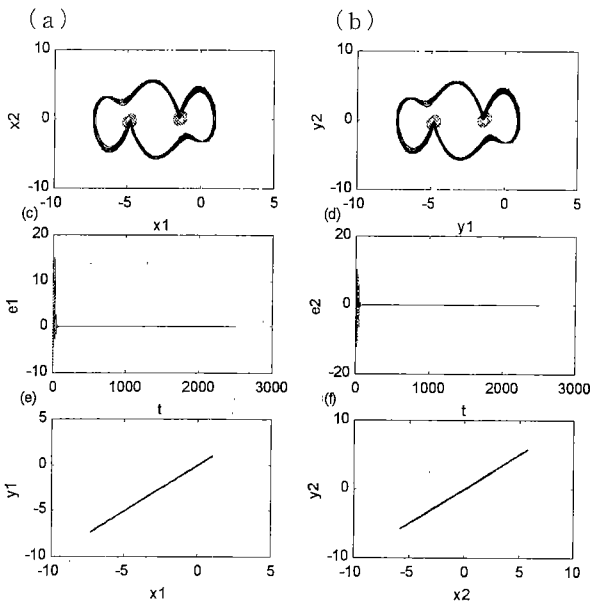

Fig. 5 (a), (b) Phase portrait, (c), (d) Time-response error and (e), (f) $x-y$ diagram by observed-based synchronization scheme

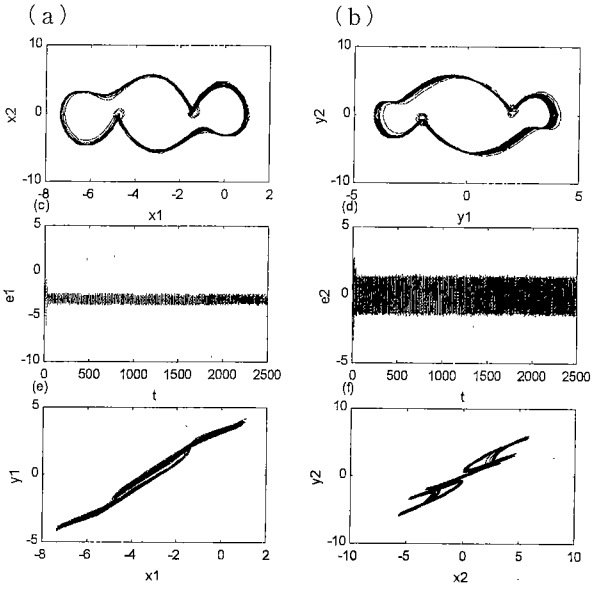

Fig. 6 (a), (b) Phase portrait, (c), (d) Time-response error and (e), (f) $x-y$ diagram by observed-based synchronization scheme

synchronized, and the error dynamics approaches to zero finally.

In the observed-based synchronization scheme, it is very important to select an appropriate substituting signal. When the signal x_1 of the drive system is used to substitute the signal y_1 of the $\sin y_1$ term of the response system, the response system becomes:

$$\begin{cases}\dot{y}_1=y_2\\ \dot{y}_2=-2\xi y_2-\sin x_1[\omega^2(\rho+\cos y_1)+\gamma\sin\omega t]\end{cases}$$

(response system) (8)

Figure 6 shows the simulated results, two systems are not synchronized. The phase portraits of two systems are not the same, and the error dynamics does not approach to zero finally.

2.4 Transient time in unidirectional synchronization

In this section, in order to analyze the influence on transient behavior of the synchronized systems by coupling strength and different initial conditions, we consider unidirectional coupled chaotic systems by adding a periodic coupling term[6]. The Euclidean distance $d=\sqrt{(x_1-y_1)^2+(x_2-y_2)^2}$ between the two trajectories is monitored for various choices of the coupling parameter k, as shown in Fig. 7 with the same initial conditions $(\theta(0), \dot{\theta}(0))=(\pi+0.02, 0.02)$. By increasing the value of the coupling parameter, the distance d approaches to zero when $k\geq 8.3$, then the two subsystems display the same output. For values of k greater than $k_{thr}=8.3$ the synchronized state is stable.

In Fig. 8, two typical curves representing the full evolution of $d(t)$, for two values of k above the synchronization threshold. Two curves are computed for identical initial conditions but $k=8.361$ and 10, so that the invariant subset has two different types of stability, and we note that the observed decay is qualitatively different. The evolution of $d(t)$ when $k=8.361$ can be notionally separated into two different parts. The first evolution (τ_0), until time approximately 180 seconds, it shows no appreciable change in the order of magnitude of the distance measure $d(t)$. After this, in the time interval τ_d, the trajectory starts to decay towards the synchronized state with relatively fast rate, and in the logarithmic scale its decay is almost linear. For the second case $k=10$, $d(t)$ becomes a monotonically decreasing function of time.

In Fig. 9, curves presenting the evolution of $d(t)$ are shown again on linear-log scale, with $k=8.361$ fixed, for three different initial conditions. More precisely $(y_1(0), y_2(0))=(0.05, 3)$ and $x_2(0)=0.02$ are kept fixed, and we use three different starting points $x_1(0)$, as given in the figure below each end of the three curves. The slope of the linearly decaying part or the decaying transient for each of the three curve is almost the same, corresponding to the intuitive conjecture that the convergence is governed by the strength of dissipation transverse to the attractor.

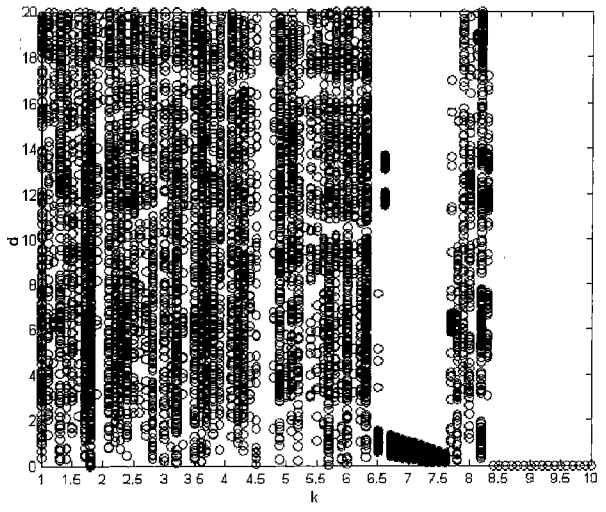

Fig. 7 Plot of several values of the Euclidean distance $d(t)$ between the trajectories $(x(t), \dot{x}(t))$ and $(y(t), \dot{y}(t))$ for different values of k. The transition to a stable synchronized state is located approximatively at $k_{th}=8.3$

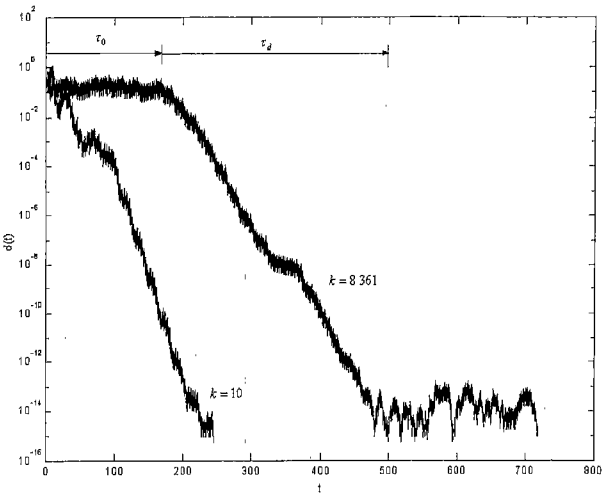

Fig. 8 Two curves representing the time evolution of the Euclidean distance $d(t)$ between the drive and the response trajectories with different coupling strength $k=8.361$, and 10

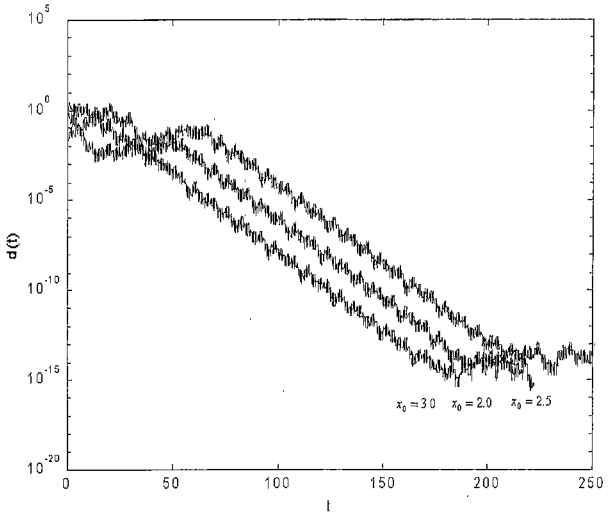

Fig. 9 The behavior of $d(t)$ for three cases of convergence onto the synchronized subset for three different initial conditions $x_0=3.0$, 2.0 and 2.5

3. Chaotic Secure Communication Systems

In recent years, using chaotic signals to address the secure communication problem has received a great deal of attention. Various methods for chaos-based secure transmission of private information signals have been proposed by several authors[10],[11]. Instead of conventional communication transmission channel, a new transmission method is adopted for the purpose of higher security in Ref.(12). Different from Ref.(12), a more complex encryption function is used in this chapter to enhance the sensitivity and security of the communication system. The chaos-based scheme for secure communication is composed of three steps: (1) Signal encryption, (2) System synchronization and (3) Signal decryption.

In the first step, a highly nonlinear function ϕ is used to encrypt both the information-bearing signal $s(t)$ and the chaotic-state signals $x(t)$. Then the message signal $s(t)$ is hidden in the encrypted signal $s_e(t)$ which is transmitted to the receiver. In the second step, the chaotic signal $h(x)$, which is in general a real-valued function of the states x of the chaotic transmitter, is transmitted in the other channel. For simplicity, $h(x)=x_1$ is used here. In the third step, we use the estimates $y(t)$ generated from the response system and the decryption function ξ to reproduce an approximate estimate $s_d(t)$ of the masked confidential signal. By synchronization of drive and response systems, recovered signal $s_d(t)$ and message signal $s(t)$ are almost the same. A schematic description of the entire process is depicted in Fig. 10. Now, we illustrate the secure communication scheme with the help of the unidirectional-coupled systems. The drive and response systems are expressed as Eqs.(4) and (5). We also take the following encryption and decryption functions:

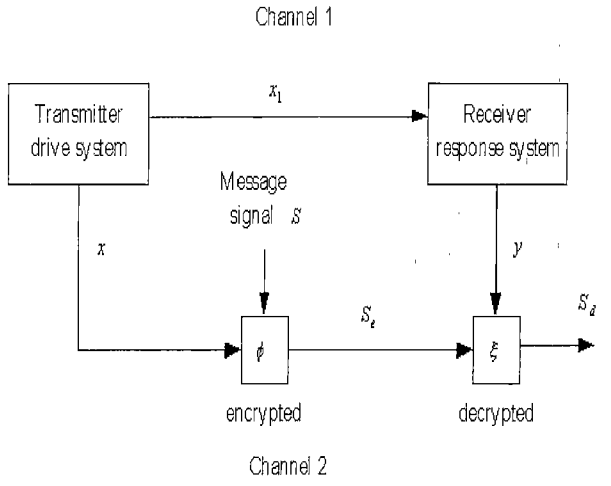

Fig. 10 The schematic process of the chaotic secure communication system

encryption function $\phi=x_2^3+(x_2+x_2^2+x_2^4)s=s_e(t)$

decryption function $\xi=-\frac{x_2^3}{(x_2+x_2^2+x_2^4)}+\frac{s_e}{(x_2+x_2^2+x_2^4)}$

which are more complex than that in Ref.(12). The message function $s(t)=0.2\sin(10\pi t)$ is hidden in the encrypted signal $s_e(t)$ and transmitted to the receiver. Then the chaotic signal x_1 of the drive system is transmitted to the response system in the other channel for synchronization. Finally decrypted signal $s_d(t)$ is recovered by the decryption function. Figure 11 shows the simulated results of encrypted and decrypted signals in the absence of the noise. By the synchronization of the drive and response systems, the decrypted signal $s_d(t)$ approaches to the information signal $s(t)$ and decrypted error $s(t)-s_d(t)$ approaches to zero.

Next, we demonstrate sensitivity of the communication system to synchronization errors made by the intruder. Assume that the intruder succeeds to intercept an approximate estimate of $x(t)$, in our case, $y_2(t)+d$ for $x_2(t)$. The error d may results in model errors. Figure 12 shows the simulation results for $d=0.01$. As seen in Fig. 12, the decrypted error $s(t)-s_d(t)$ is so significant that the recovered signal $s_d(t)$ is quite different from the message signal $s(t)$.

From Figs. 11 and 12, it shows us that using a highly nonlinear encryption function, involving all chaotic states, can yield strong sensitivity to the encrypted error and therefore guarantee higher security and privacy.

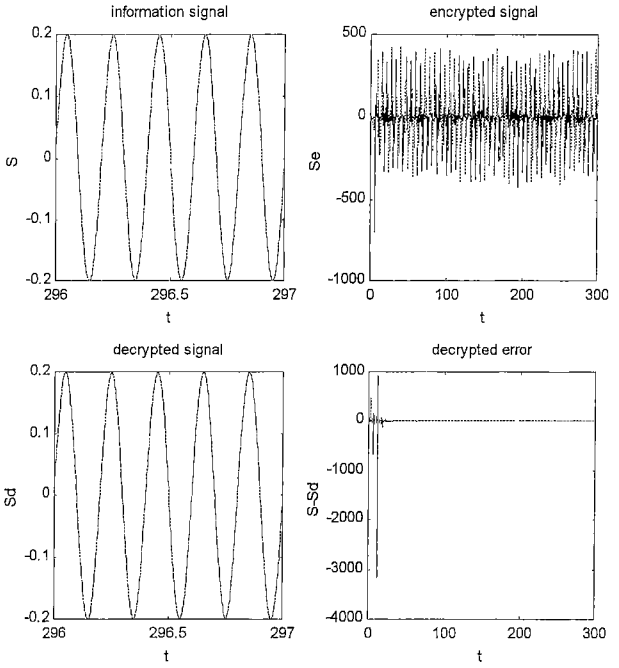

Fig. 11 The information signal $s(t)$, encrypted signal $s_e(t)$, decrypted signal $s_d(t)$, and decrypted error $s(t)-s_d(t)$

4. Anticontrol of Chaos

Anticontrol of chaos, in contrast to the controlling of chaos, is to make a non-chaotic dynamical system chaotic or enhance the existing chaos of an originally chaotic system. It has attracted attention in recent years due to its great potential applications such as in the field of physical, mechanical, electrical, optical and biological system[13),(14)].

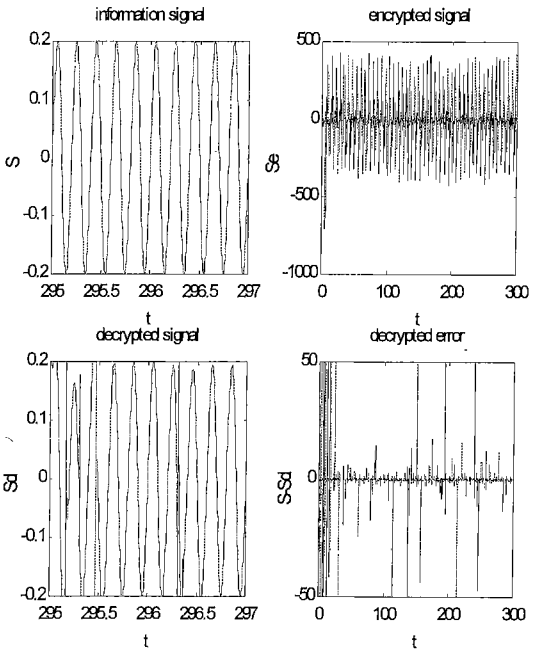

Fig. 12 Sensitivity of the secure communization system for $d=0.01$

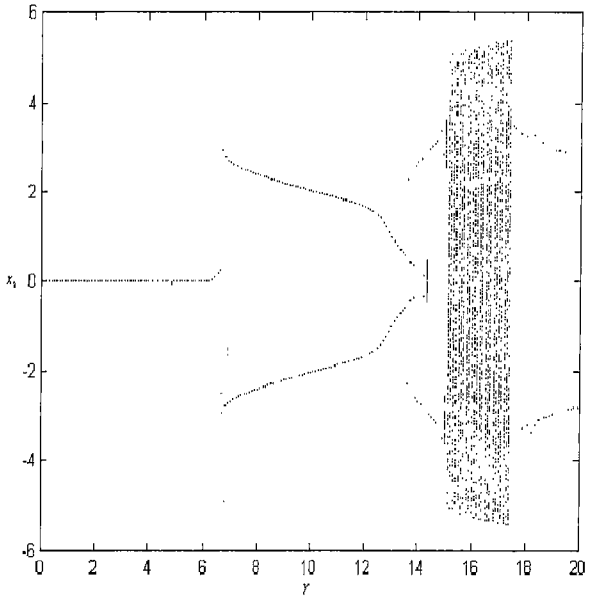

Fig. 13 Bifurcation diagram versus γ of the original system

4.1 Anticontrol of chaos by adding constant term

The first method to control system dynamics from periodic motion to chaos is adding a negative constant term T. Equation (3) can be rewritten as

$$\begin{cases}\dot{x}_1=x_2\\ \dot{x}_2=-2\xi x_2-\sin x_1[\omega^2(\rho+\cos x_1)+\gamma\sin\omega t]-T\end{cases} \quad (9)$$

where T is constant. Figure 13 shows bifurcation diagram of the original system in Eq.(3). The system is chaotic when $\gamma=14.3$ and $15.1\leq\gamma\leq17.4$. Figure 14 shows the bifurcation diagram of the system in Eq. (9) for $T=0.8$. The periodic motion becomes chaos within more parameter ranges. Figure 15 shows the Lyapunov exponent corresponding to Fig. 14. The

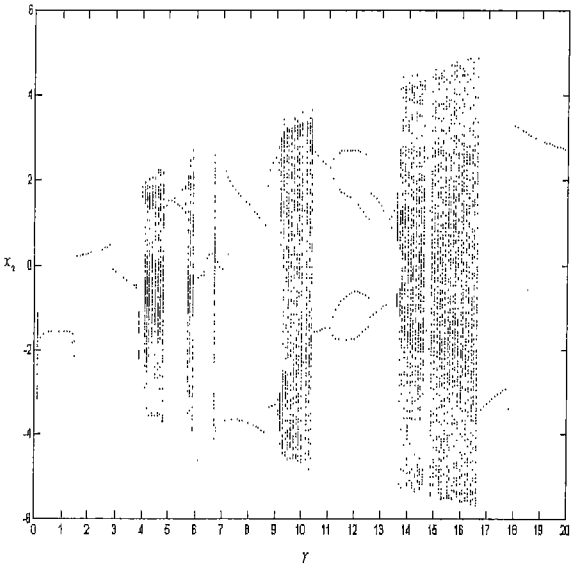

Fig. 14 Bifurcation diagram versus γ of the adding negative constant term system for $T=0.8$

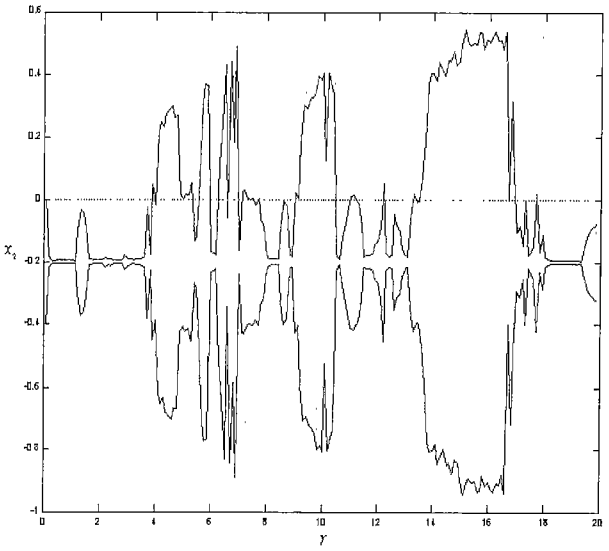

Fig. 15 The Lyapunov exponent versus γ of the adding negative constant term system for $T=0.8$

Lyapunov exponent is positive in chaotic range. To see the trend from order to chaos, we vary the parameter value ρ and negative constant term T and record that range of chaos γ in the bifurcation diagram. A three-dimensional diagram is showed in Fig. 16.

4.2 Anticontrol of chaos by adding periodic term

We can also control the system from order to chaos by adding a negative periodic term. The system can be rewritten as:

$$\begin{cases} \dot{x}_1 = x_2 \\ \dot{x}_2 = -2\xi x_2 - \sin x_1[\omega^2(\rho + \cos x_1) + \gamma \sin \omega t] \\ \quad - T \sin \omega_1 t \end{cases} \tag{10}$$

where $\omega_1 = 2.5$. Figure 17 shows the bifurcation diagram versus γ of system in Eq. (10) for $T = 3.0$. When T becomes large, the system behaves from regular motion to chaos. Figure 18 shows the Lyapunov exponent corresponding to Fig. 17.

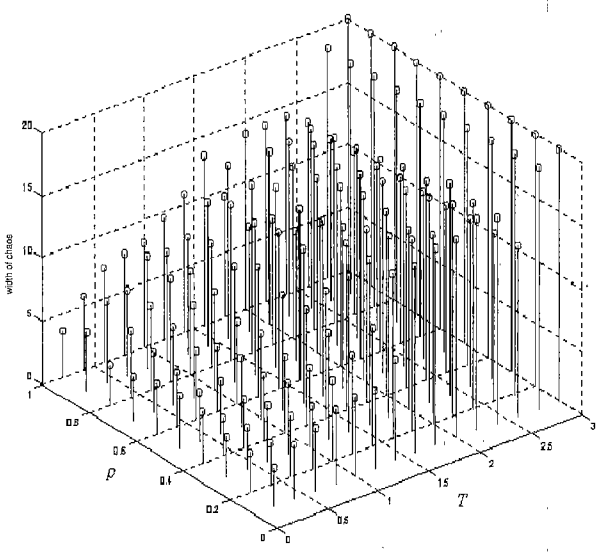

Fig. 16 A three-dimensional diagram for ρ, T and the width of chaotic range

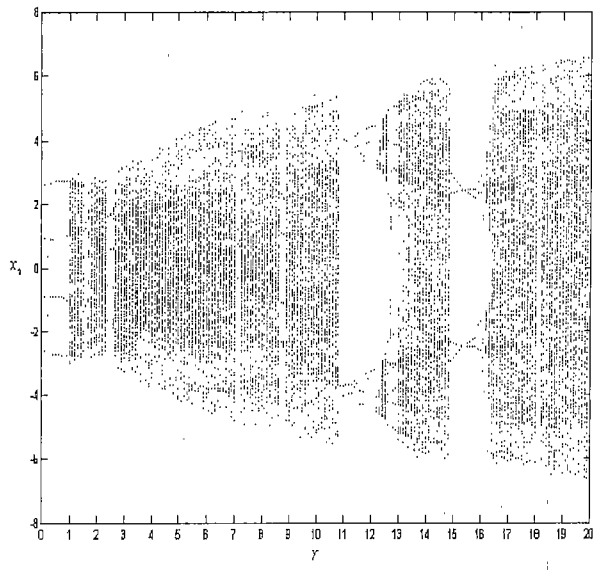

Fig. 17 The bifurcation diagram versus γ of the adding negative periodic term system for $T = 3.0$

4.3 Anticontrol of chaos by adding periodic impulse term

Like section 4.2, the system also can be added by a periodic impulse term instead of a periodic term. The system becomes:

$$\begin{cases} \dot{x}_1 = x_2 \\ \dot{x}_2 = -2\xi x_2 - \sin x_1[\omega^2(\rho + \cos x_1) + \gamma \sin \omega t] \\ \quad - T \sum_{j=0}^{\infty} \delta(t - jk_p) \end{cases} \tag{11}$$

where T is a constant impulse intensity, k_p is the period between two consecutive impulse, and δ is standard delta function. Figure 19 shows the simula-

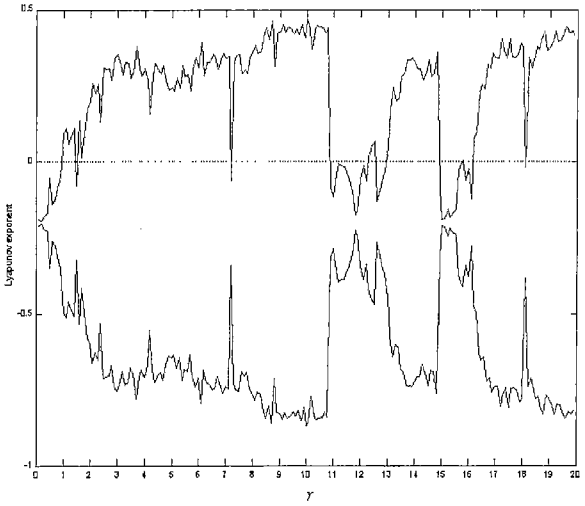

Fig. 18 The Lyapunov exponent versus γ of the adding negative periodic term system for $T = 3.0$

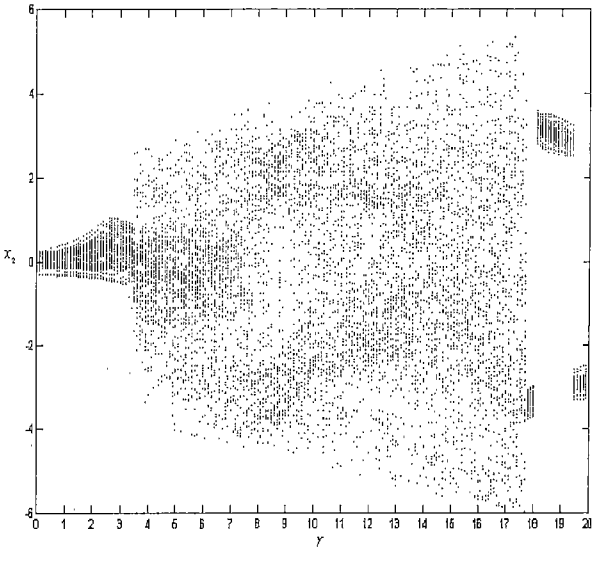

Fig. 19 The bifurcation diagram versus γ of the adding negative impulse term system for $T = 1.0$ and $k_p = 20.5$

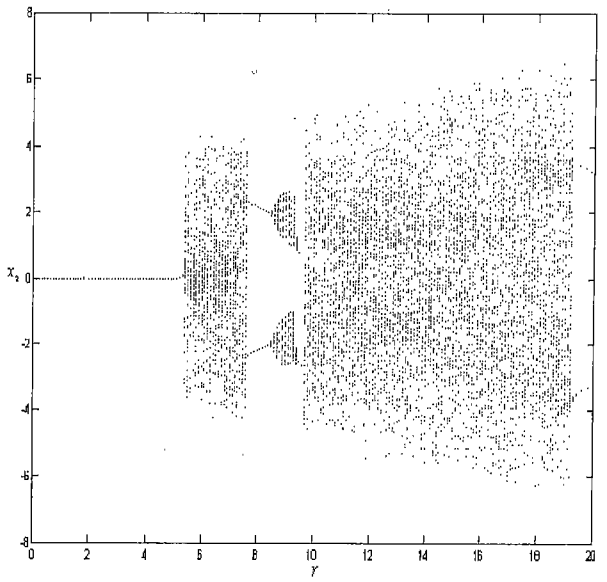

Fig. 20 The bifurcation diagram versus γ of the adding delay time feedback term system for $T=0.3$ and $\tau=10$

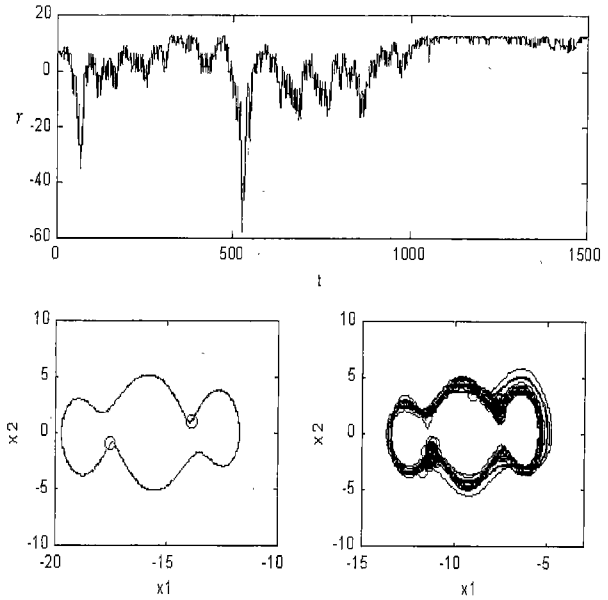

Fig. 21 From period-2 to chaos by adaptive control

tion result of bifurcation diagram. When $k_p=20.5$ and $T=1.0$, the chaotic range increases.

4.4 Anticontrol of chaos by adding delay feedback term

In this section, a delay nonlinear (or linear) feedback function is added[15]. The system can be rewritten as:

$$\begin{cases} \dot{x}_1=x_2 \\ \dot{x}_2=-2\xi x_2-\sin x_1[\omega^2(\rho+\cos x_1)+\gamma \sin \omega t] \\ \quad -Tu(x(t-\tau)) \end{cases} \tag{12}$$

where T is a constant, u is the delay feedback function, τ is delay time. Here, a simplest function $u=x_1(t-\tau)$ is used. Figure 20 shows the simulation result of bifurcation diagram when $T=0.3$ and $\tau=10$.

4.5 Adaptive control

An adaptive control algorithm is a control method utilizing an error signal proportional to the difference between the goal output and actual output of the system[15]. Generally speaking, an adaptive controller is one that has adjustable parameters and the capability of self-adjusting these parameters in response to changes within the dynamics and environment of the controlled system. The system motion is set to the desired state x_s by adding dynamics on control parameter R through the evolution equation:

$$\dot{R}=Au(x-x_s) \tag{13}$$

where u is a suitable function, and A is the stiffness of control. In order to control the system in Eq.(3) from periodic motion to desired chaotic motion x_s, we choose the parameter γ perturbed as:

$$\dot{\gamma}=A(-(x_1-x_{1s})\times(x_2-x_{2s})) \tag{14}$$

where $A=0.025$. Figure 21 shows the simulation result. We control the system from period-2 to chaos.

5. Conclusions

Synchronization of two or more dynamical systems is a fundamental phenomenon for studying in the physical, mechanical, electrical, optical and biological field. In this paper, chaos synchronization and chaos anticontrol of a rotationally supported simple pendulum are researched by some methods. In Chapter 2, chaos synchronization is achieved by feedback-based and observed-based scheme. In Chapter 3, we utilize a new communication system to accomplish the application of chaos synchronization. In Chapter 4, anticontrol of chaos is achieved by adding different kinds of terms. We can make the Lyapunov exponent of the control system positive in more range. Finally, adaptive control is also adopted to control the system from order to chaos.

Acknowledgments

This research was supported by the National Science Council, Republic of China, under Grant Number NSC 92-2212-E-009-027.

References

(1) Kapitaniak, T., Controlling Chaos, (1996), Academic Press, London.

(2) Mosekilde, E., Complexity, Chaos and Biological Evolution, Nato Series, (1991), Plenum, New York.

(3) Strogatz, S.H., Nonlinear Dynamics, and Chaos, (1994), Addison, Reading.

(4) Terry, J.J. and VanWiggeren, G.D., Chaotic Communication Using Generalized Synchronization, Chaos Solitons and Fractals, Vol. 12 (2001),

pp. 145-152.
(5) Sarasola, C., Torrealdea, F.J., d'Anjou, A. and Grana, M., Synchronization of Non-Identical Chaotic Systems, Control of Oscillations and Chaos, 2000 Proceedings. 2000 2nd International Conference, Vol. 3 (2000), pp. 475-479.
(6) Santobont, G., Bishop, S.R. and Varone, A., Transient Time in Unidirectional Synchronization, International Journal of Bifurcation and Chaos, Vol. 9, No. 12 (1999).
(7) Murali, K. and Lakshmanan, M., Secure Communication Using a Compound Signal from Generalized Synchronicale Chaotic Systems, Physics Letters A, Vol. 241 (1998), pp. 303-310.
(8) Vadivasova, T.E., Balanov, A.G., Sosnovtseva, O.V., Postnov, D.E. and Mosekilde, E., Synchronization in Driven Chaotic Systems: Diagnostics and Bifurcations, Physics Letters A, Vol. 253 (1999), pp. 66-77.
(9) Paul, R.S., Rajasekar, S. and Murali, K., Coexisting Chaotic Attractors, Their Basin of Attractions and Synchronization of Chaos in Two Coupled Duffing Oscillators, Physics Letters A, Vol. 264 (1999), pp. 283-288.
(10) Corron, N.J. and Hahs, D.W., A New Approach to Communications Using Chaotic Signals, IEEE Trans. Circuits Syst. I, Vol. 44 (1997), pp. 373-382.
(11) Liu, Y., Chen, H.F., Liu, J.M., Davis, P. and Aida, T., Communication Using Synchronization of Optical-Feedback-Induced Chaos in Semiconductor Lasers, Circuits and Systems I: Fundamental Theory and Applications, IEEE Transactions on, Vol. 48, Issue: 12 (2001), pp. 1484-1490.
(12) Jiang, Z.P., A Note on Chaotic Secure Communication Systems, Circuits and Systems I: Fundamental Theory and Applications, IEEE Transactions on, Vol. 49, Issue: 1 (2002), pp. 92-96.
(13) Chen, G., Control and Anticontrol of Chaos, Control of Oscillations and Chaos, 1997. Proceedings, 1997 1st International Conference, Vol. 2 (1997), pp. 181-186.
(14) Chen, G. and Lai, D., Anticontrol of Chaos via Feedback, Decision and Control, Proceedings of the 36th IEEE Conference on, Vol. 1 (1997), pp. 367-372.
(15) Chen, G. and Dong, X., From Chaos to Order, (1998), p. 177, p. 335, World Scientific, New Jersey.